A field study on the effects of fines on the interpretation of CPTu

An-Bin Huang
National Chiao Tung University, Dept. of Civil Engineering, Taiwan, huanganbin283@gmail.com

Anders Hust Augustesen[1], Caspar Thrane Leth[2],
Edward Charles George Molyneaux[3], Lone Krogh[4],
Ørsted Offshore, Gentofte, Denmark
andau@orsted.dk[1], xcaet@orsted.dk[2], edmol@orsted.dk[3], lonkr@orsted.dk[4]

ABSTRACT: The soils in the offshore windfarm areas along the West Coast of Taiwan consist of a mixture of fine sand with various amounts of fines. The fines can be silt or clay and be more dominant than sand and CPTu in these soil deposits can be partially drained. The partial drainage poses challenges to the interpretation of CPTu especially when the CPTu is the primary tool for site characterization and determination of engineering properties in relation to design of offshore wind turbine foundations. Most of the available interpretation methods consider either the CPTu as fully drained or undrained. A field study was carried out at a test site where a series of CPTu with varying rates and high quality undisturbed soil samples were taken with gel-push sampler. Laboratory element tests on undisturbed samples were conducted. Based on these tests, a method that uses soil behavior type index to quantify or filter the effects of partial drainage is proposed. This paper details the geological background of the test site, field/laboratory tests conducted and discusses the implications in the interpretation of CPTu considering the effects of partial drainage.

Keywords: cone penetration test; gel-push sampling; soil behavior type index; partial drainage; undrained shear strength

1. Introduction

Large scale offshore wind power projects developed along the West Coast of Taiwan. Available subsurface explorations in this area have indicated transitional soils that consisted mostly of fine sand with various amounts of fines (particles passing ASTM #200 sieve) in a form of silt or clay. According to earlier studies [1][2], the sand/fines soil on the West Central Coast of Taiwan contain Mica. The sand grain sized Mica is platy and relatively compressible or low in dilatancy which must be considered when encountered. Cone Penetration Test with pore pressure measurement (CPTu) is the principal tool in site characterization in the design for offshore wind turbine foundations. Due to variable nature of the fines contents in this type of transitional soil, identification of drainage conditions is imperative for proper interpretation of the CPTu. An onshore study campaign was carried out with the purpose to establish a methodology in the identification of drainage conditions from CPTu in the sand/fines soil. The study also aimed at providing a baseline knowledge in the determination of soil stress history, compressibility, undrained shear strength from CPTu with proper consideration of drainage conditions and soil characteristics.

1.1. The test site and study program

An onshore test site at the west coast of Taiwan with identified transitional soils, cf. Fig. 1, was available for the study campaign. The site was part of a land reclamation project completed in the 1980's. The top 10 m of soil was expected to be fill placed during the land reclamation. The ground surface is at 3.7 m above the mean sea level. The groundwater table was at 2 to 3 m below the ground surface. The field soil testing and sampling were distributed in three cluster locations as shown in Fig. 1 where all test denominations presented in this paper refer to the three cluster names. The testing and sampling concentrated in the depth range between 10 and 30 m. Five profiles of CPTu with various configurations, one profile of PressureMeter Test (PMT), and Lugeon test were conducted at each cluster location. The PMT and Lugeon test results will not be reported herein. A series of undisturbed gel-push soil samples [3] were taken at each cluster location. The in situ tests and soil sampling boreholes at each cluster location were restricted within a 3 m radius circle. No two tests or sampling locations were spaced less than 1 m apart.

Figure 1. The test site and borehole cluster locations diagram.

A profile of gel-push sampling was conducted at the center of each cluster location. Samples were taken from 10 to 30 m below ground surface at 1.5 m intervals. The gel-push samples have a diameter of 73 mm and a length of 1 m. It has been demonstrated that the gel-push sampler can provide high quiality, low disturbance soil samples [3]. The undisturbed gel-push samples were used to perform one-dimensional oedometer, Rowe cell, direct simple shear and K_o consolidated triaxial compression

tests. Except for a few samples of clean sand, the shearing tests were conducted undrained. The consolidation tests provided compressibility measurements in the vertical and radial directions. These values were used in the evaluation of CPTu data and application of the concept of normalized velocity. The laboratory tests on the high quality gel-push soil samples provided reference values in grain size distribution, stress history and strength for the interpretation of CPTu.

2. Geological origin and soil properties

Parts of the Western and Southern Taiwan are covered by a thick deposit of alluvial material. The upper soil layers in the project area were deposited in the Holocene epoch. The alluvial material originated from the central mountain range that lies on the east side of Taiwan in a north-south direction. Earthquakes weakened the rock formations in the central mountain range which were mostly sedimentary and metamorphic in nature. Rainfalls created landslides and debris flows, the eroded debris eventually deposited and formed the land on the west side of Taiwan. The process of transportation by rapidly flowing streams ground the fractured rock into sand and fines particles before deposition on the west plain, to a thickness of several hundred meters.

The general stratification at the test site consists of 8-13 m fill, 5-15 m highly stratified mixture of fine sand, silts and clays above a layer predominated of sand.

Fig. 2 shows the grain size distribution curves taken from the available gel-push samples. The majority of the soil samples had grain sizes in the silt and clay range. The wide variation of fines content is evident in Fig. 3. Only samples from below 27 m had fines consistently less than 20%. The sand grains had diameters mostly less than 0.5 mm. Significant parts of the soil samples were non-plastic. The available Atterberg limit test data shown in Fig. 4 had most of the plasticity index ranged from 8 to 15. The specific gravity of soil grains was mostly around 2.70. A separate mineralogy study was carried out to verify the Mica content. No significant amount of Mica was found in the sand fraction of the soil specimens taken from this test site, thus the influence of Mica on soil behavior is considered insignificant for the present study.

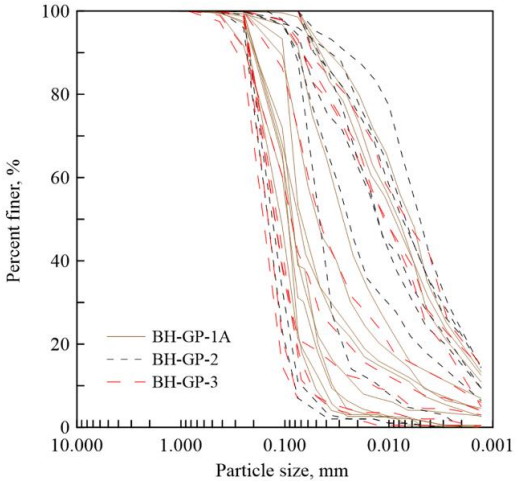

Figure 2. Grain size distribution curves from available gel-push samples.

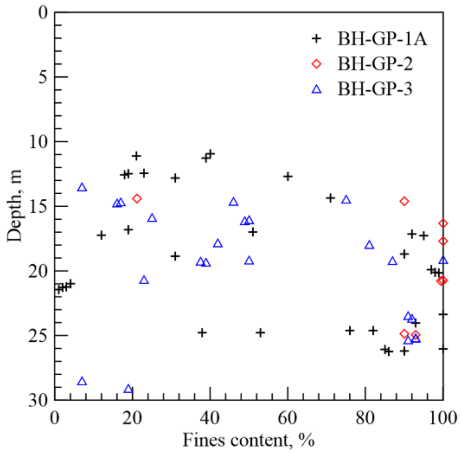

Figure 3. Fines contents versus depth.

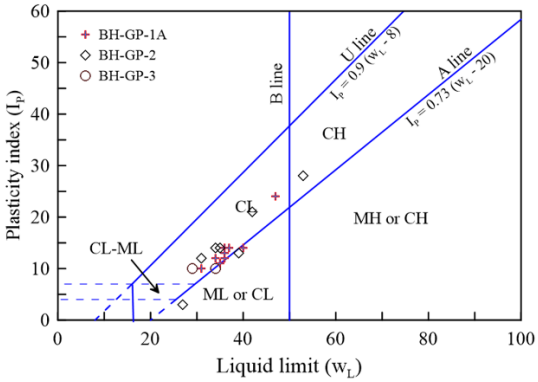

Figure 4. Available Atterberg limit test results.

3. Reference laboratory tests

A series of laboratory tests on intact gel-push samples were caried out to provide reference parameters related to soil compressibility, stress history, strength and rigidity index. These laboratory tests included consolidation tests, direct simple shear and K_o consolidated triaxial compression tests. All test specimens to be reported here were trimmed down to diameters less than 73 mm. When extruding specimens from the sampling tube, a trimmer was used to remove the excess soil and fit the specimen to the required diameter. The specimen trimming also cut off the thin layer of soil that was contaminated by the lubricant gel injected during sampling. The following sections describe the trends of the results of the reference tests.

3.1. Consolidation tests

The aim of this series of tests was to provide a profile of pre-consolidation stress and coefficients of consolidation in vertical and radial or horizontal directions. Step loading one dimensional consolidation or oedometer tests (ASTM D 2435) and Rowe cell tests (BS 1377-6) were performed. In both types of consolidation tests, the specimen was preloaded to the expected field effective overburden stress, σ'_{vo} and then released the preloading before proceeding to the consolidation test in order to evaluate sample disturbance. In oedometer tests, the specimen (60.5 mm diameter and 20.0 mm height) was allowed to drain from top and bottom. The Rowe cell tests used an equal strain procedure where the vertical

stress (66.8 mm diameter and 33.0 mm height) was applied with a rigid plate. A radial to periphery drainage condition was applied. Pore pressure was measured at the base center under back pressure. The obtained pre-consolidation stress would correspond to unusually large overconsolidation ratio (OCR) that is not compatible to the young age of the tested soil deposit and there is no history of large scale mechanical pre-loading. Likely due to the sandy/silty nature of the specimens, no meaningful or consistent pre-consolidation stress could be identified from either type of consolidation test results.

Fig. 5 plots the coefficient of consolidation in vertical direction, c_v from oedometer tests and coefficient of consolidation in radial direction, c_{ro} from Rowe cell tests. These values were taken at the end of preloading and the effective vertical consolidation stress was close to the field overburden stress, σ'_{vo}.. c_{ro} scattered much more than c_v, and c_{ro} can be two orders of magnitude larger than c_v at similar depth. Drainage in the vertical direction is dominated by the presence of low permeable layers while permeable layers tend to influence drainage in the radial direction. In addition to anisotropy of compressibility, the layered nature of the alluvial deposit is likely the cause for the differences between c_v and c_{ro}.

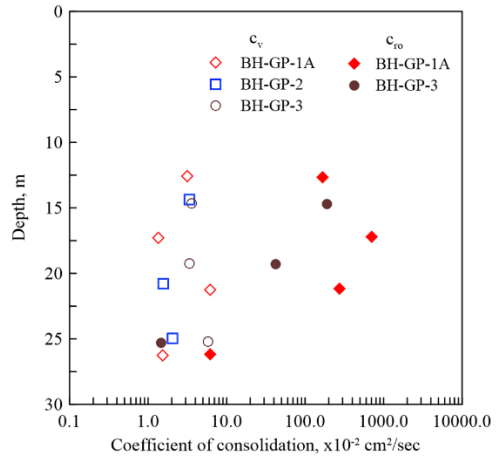

Figure 5. Coefficients of consolidation from oedometer and Rowe cell tests.

3.2. Shearing tests

The shearing tests included monotonic triaxial (TX) and direct simple shear (DSS) tests on intact samples. The TX specimen was 70mm in diameter and 140mm high. All TX tests reported herein were K_o consolidated undrained compression (CKoUc) tests (ASTM D4767-11). Three to five CKoUc tests were carried out on samples taken from each borehole cluster. The specimens were consolidated under K_o condition to an effective vertical stress, σ'_v equal to the field effective overburden stress, σ'_{vo}. The specimens were then sheared undrained under a constant horizontal stress, σ_h derived at the end of K_o consolidation. Figs. 6a and 6b show relationships among deviator stress $(\sigma'_v - \sigma'_h)$, excess pore pressure and axial strain, and stress paths p' $(=(\sigma'_v + \sigma'_h)/2)$ versus q $(=(\sigma'_v - \sigma'_h)/2)$ on BH-GP-2 samples as an example (σ'_h = effective horizontal stress). In most cases, the shearing induced positive excess pore pressure before reaching a stable value or decreasing to negative range. For the tests shown in Fig. 6, distinctive dilative behavior, often found in shearing tests on clean quartz sand, was noticed only in the test on specimen from 24.86 m, where-as three tests showed initial dilative behaviour. The undrained shear strength, s_{u-TX} was taken as the peak q in the TX test. As shown in Fig. 7, the available s_{u-TX} values ranged from 50 to 350 kPa and generally increased with depth.

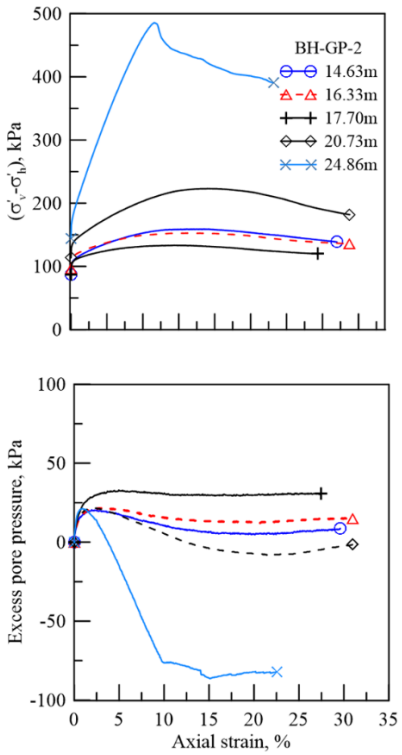

Figure 6a. Stress, excess pore pressure and strain relationships of TX from BH-GP-2. Legend refer to sample depth.

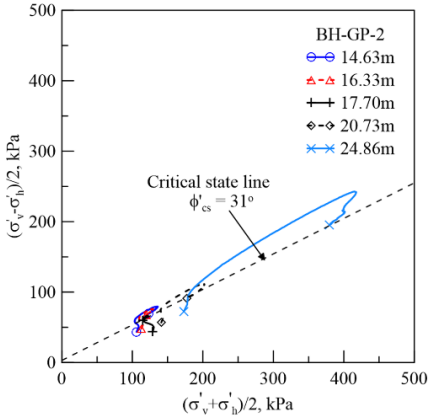

Figure 6b. Effective stress paths of TX from BH-GP-2. Legend refer to sample depth.

Rigidity index is an important parameter used in the interpretation of in situ tests, such as determination of coefficient of consolidation or OCR from CPTu and undrained shear strength from PMT especially when the cavity expansion theory is involved. The TX and DSS tests provided a series of data where the rigidity index can be evaluated using tests on undisturbed samples. The rigidity index, I_r is taken as G_{50-TX}/s_{u-TX} where G_{50-TX} is the secant shear modulus at 50% of the peak deviator stress. The obtained I_r ranged from 3.4 to 19.4. The critical state friction angles, $\emptyset'_{cs}$ from all the TX tests

ranged from 29° to 34°. The range of $\emptyset'_{cs}$ is compatible to the values reported earlier for soils in the region [4]. The variation of $\emptyset'_{cs}$ apparently relates to grain size differences. For the TX tests shown in Fig. 6 the effective peak friction angle, $\emptyset'_{peak}$ ranged from 33.5° to as much as 38°. A general trend is that the lower fines contents correspond to higher $\emptyset'_{cs}$ and higher $\emptyset'_{peak}$.

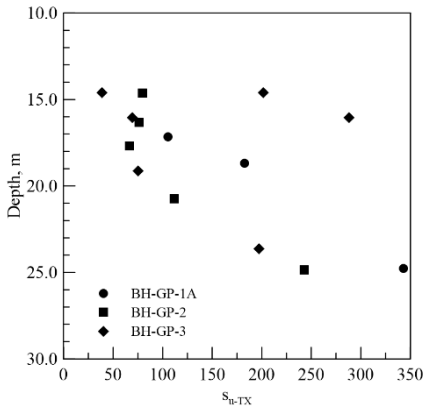

Figure 7. Undrained shear strength s_{u-TX} from TX versus depth.

The Direct Simple Shear (DSS) specimen (70.0 mm diameter and 20.0 mm height) was consolidated to the field overburden stress and then sheared undrained. The static or monotonic DSS followed ASTM D 6628 with a strain rate of 4 to 5%/hr. The shearing was conducted under a constant volume condition. The specimen was contained in stacked rings that prevented lateral strain during shearing. The vertical stress was monitored while keeping the specimen height fixed (i.e., vertical strain = 0). The change in vertical stress was taken as the shear induced excess pore pressure.

Five to eight DSS were conducted on samples from each each borehole cluster. As in the case of TX, DSS shearing induced positive excess pore pressure before reaching a stable value or decreasing to the negative range. Figs. 8a and 8b show relationships among shear stress, τ, excess pore pressure and shear strain γ and stress paths of σ'_v versus τ of DSS tests on BH-GP-1A samples as an example. The undrained shear strength, s_{u-DSS} was taken as the peak τ in the DSS test. As shown in Fig. 9 the available s_{u-DSS} values ranged from 50 to 200 kPa. s_{u-DSS} decreases with depth first to approximately to 17 m and then increased with depth.

For DSS, I_r is defined as G_{50-DSS}/s_{u-DSS} where G_{50-DSS} is the secant shear modulus taken at 50% of the peak shear stress. The obtained I_r ranged from 4.8 to 12.5, comparable to those from TX described above. The I_r values from TX and DSS correspond to I_r of clays with overconsolidation ratios (OCR) higher than 5 and plasticity indices over 50 [5].

Twelve pairs of DSS and TX at similar depths can be identified. The ratio of s_{u-DSS}/s_{u-TX} at similar depths ranged form 0.21 to 1.52 with an average of 0.62. This ratio is surprisingly close to s_{u-DSS}/s_{u-TX} of 0.61 reported for Boston Blue clay [6]. To facilitate evaluation of the stress history profile of the soil deposit, a plot of undrained shear strength normalized with respect to the applied effective vertical consolidation stress or overburden stress, σ'_{vo} from TX and DSS with depth was made. A ratio of s_{u-DSS}/s_{u-TX} = 0.62 was used to convert s_{u-TX} to the equivalent s_{u-DSS}. A plot of "unified" s_{u-DSS}/σ'_{vo} versus depth from all TX and DSS in Fig. 10 shows a gradual decrease of s_{u-DSS}/σ'_{vo} from approximately 1 to 0.4 as the depth increases from 10 to 20 m. The decreasing trend is more obvious for s_{u-DSS}/σ'_{vo} than s_{u-TX}/σ'_{vo}. The ratio of s_{u-DSS}/σ'_{vo} remained roughly constant from below the depth of 20m. According to [7],

$$\frac{s_{u-TX}}{\sigma'_{vo}} = \frac{M}{2}\left(\frac{OCR}{2}\right)^{\Lambda} \quad (1)$$

where M is the slope of the critical state line:

$$M = \frac{6sin\emptyset'_{cs}}{3-sin\emptyset'_{cs}} \quad (2)$$

Λ is the plastic volumetric strain ratio and OCR is the overconsolidation ratio.

Take $\emptyset'_{cs}$ = 30°, Λ = 0.8 and s_{u-DSS}/s_{u-TX} = 0.62, s_{u-DSS}/σ'_{vo} = 0.4 corresponds to OCR = 2.3 and OCR ≈ 7 when s_{u-DSS}/σ'_{vo} = 1.

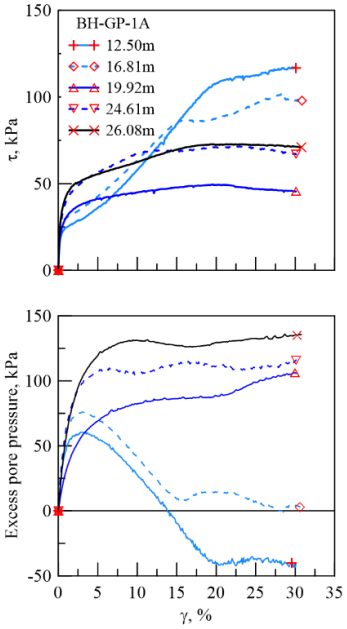

Figure 8a. Relationshps among τ, excess pore pressure and γ of DSS tests on BH-GP-1A samples'

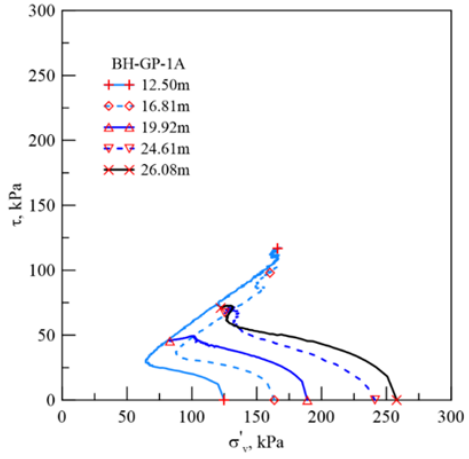

Figure 8b. σ'_v versus τ of DSS tests on BH-GP-1A samples'

This trend, albeit approximate, reflects a soil stress history that varied from overconsolidated at 10 m depth, the original ground surface prior to land reclamation, to a lightly overconsolidated state at depths beyond 20 m.

The early land reclamation construction activities and fluctuation of tidal waves may be responsible for the overconsolidation of the soil near the original ground surface.

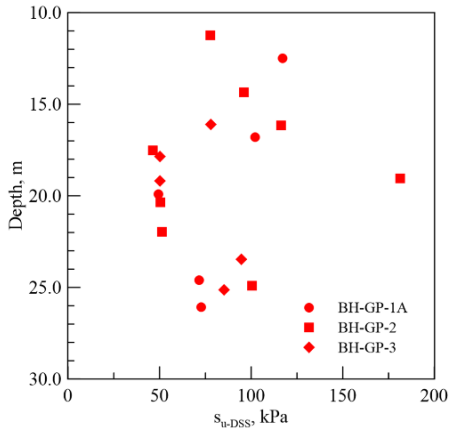

Figure 9. Undrained shear strength s_{u-DSS} from DSS versus depth.

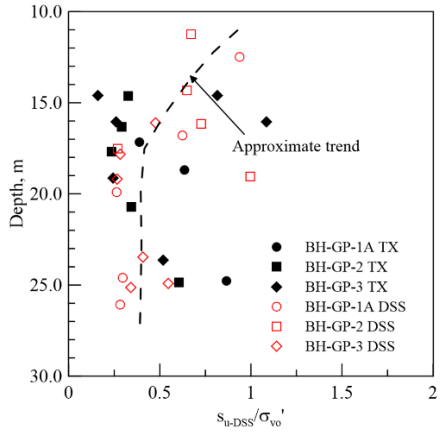

Figure 10. Unified s_{u-DSS}/σ_{vo}' versus depth.

4. Cone penetration tests

A standard 10 cm^2 cone (ASTM D-5778) was used for the study. The pore pressure element was located at u_2 position. Table 1 shows the different configurations applied in the five types of cone penetration tests at each cluster location. All CPTu were extended from ground surface to 30 m below ground surface. The rate of cone penetration, v_p varied from > 50 mm/s to lower than 5 mm/s. Pore pressure dissipation tests and seismic shear wave velocity measurements (SCPT) were made in some of the cone penetration tests. No seismic shear wave test results will be discussed herein. The various CPTu configurations were applied to reveal the existence and effects of penetration rate, partial drainage, in addition to basic soil properties. Only data from 10 m to 30 m, in the natural soil deposit, will be of interest. The CPTu A was taken at 1 m away from the gel-push borehole at all three cluster locations.

Fig. 11 shows the profiles of CPTu A from three cluster locations (BH-GP-1A, BH-GP-2 and BH-GP-3). The profiles in terms of soil behavior type index, I_C, cone tip resistance, q_t, sleeve friction ratio f_s/q_t, and pore pressure readings, u_2 were rather consistent among the three test locations. The I_C was consitently higher than 2 at depth range from 10 to 30 m. The significant zigzagging of f_s/q_t and u_2 reflects the layered nature of the aluvial soil deposit, espeically from 17.5 m to 26 m. Fig. 12 shows the profiles of A, B and E CPTu's from BH-GP-1A. Fig. 13 depicts classiciation of the same group of CPTu shown in Fig.12 by Robertson's method [8], and

$$Q_{tn} = \left(\frac{q_t - \sigma_{vo}}{p_a}\right)\left(\frac{p_a}{\sigma_{vo}'}\right)^n \quad (3)$$

$$F_r = [f_s/(q_t - \sigma_{vo})]100(\%) \quad (4)$$

where

σ_{vo} = total overburden stress

p_a = atmospheric pressure

u_o = field hydrostatic pressure

$$n = 0.381 \cdot I_C + 0.05 \cdot (\sigma_{vo}'/p_a) - 0.15 \quad (5)$$

$$I_C = \sqrt{(3.47 - logQ_{tn})^2 + (1.22 + logF_r)^2} \quad (6)$$

n was iteratively determined using Eqs. (3) to (6), and $0.5 \leq n \leq 1.0$. The data points in Fig.13 concentrate in zones 3, 4 and 5 indicating the types of soils changed from clays, to silt and sandy mixtures. This is compatible to the basic soil property tests described above. The penetration rates did not appear to have significant effects on the soil classification shown in Fig. 13.

Table 1. Configurations of cone penetration tests at each cluster.

CPTu ID	v_p, mm/s	Dissipation test		SCPT	
		Depth, m	Interval, m	Depth, m	Interval, m
A	≈20	4-30	1	10-30	1
B	≥50	11–27.5	1.5	--	--
C	≈20	11–27.5	1.5	10–27.5	1.5
D	≈20	11–27.5	1.5	--	--
E	≤5*	--	--	--	--

*: Peneteration rate, v_p ≤5 mm/s applied at 14 – 18 m and 20 – 26 m, the rest of CPTu conducted at 20 mm/s

Fig.14 shows the classification using $U-Q$ and F−Q according to the charts by Schneider et al. [9], and

$$Q = \frac{(q_t - \sigma_{vo})}{\sigma_{vo}'} = \frac{q_{tn}}{\sigma_{vo}'} \quad (7)$$

$$U = \frac{(u_2 - u_o)}{\sigma_{vo}'} = \frac{\Delta u_2}{\sigma_{vo}'} \quad (8)$$

Table 2 summarizes the 5 zones and corresponding soil types associated with the chart. According to the $U-Q$ chart shown in Fig. 14a, most of the data points fell into zone 3 or 1a/3, classified as silts and transition soils according to Table 2. When Q was high, the classification fell at the border between zones 2 (drained sands and sand mixtures) and 3. Penetration rate had no significant effect on classification according to F−Q chart shown in Fig.14b. A good portion of data points fell into zone 1b (clays) in the F−Q chart. This is similar to the Robertson's classification shown in Fig. 13.

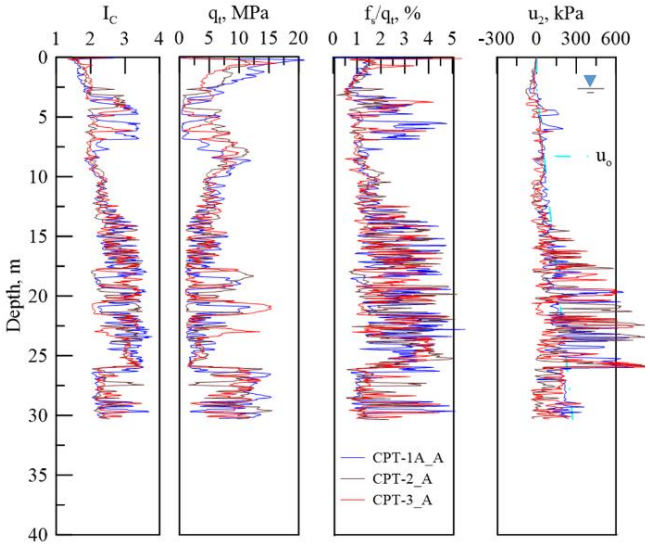

Figure 11. Profiles of A type CPTu from three cluster locations.

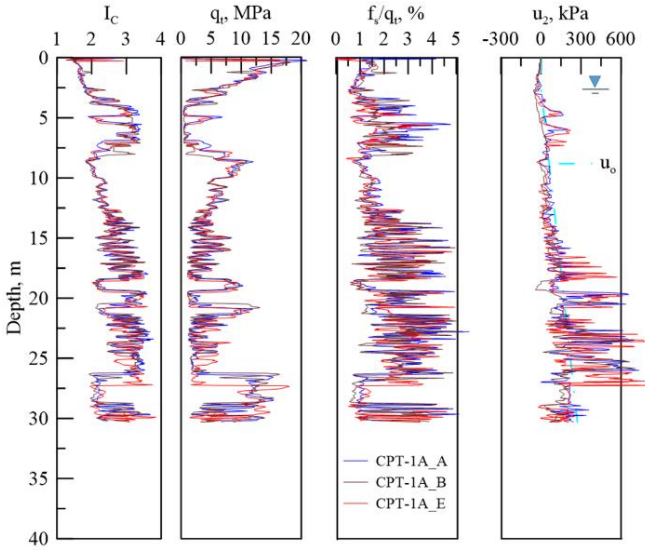

Figure 12. Profiles of A, B and E type CPTu from cluster BH-GP-1A.

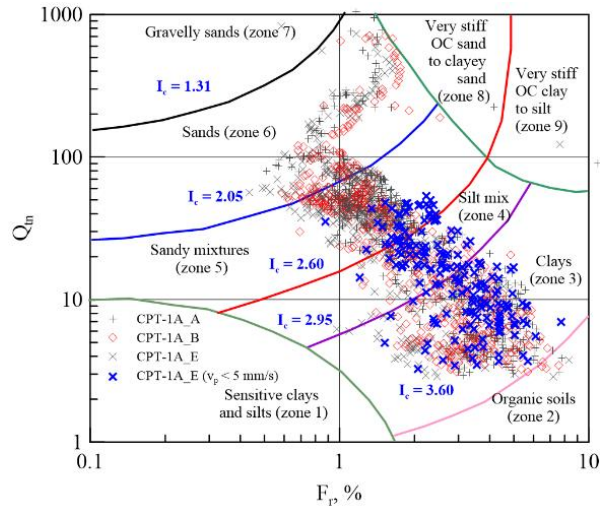

Figure 13. Classiciation of A, B and E type CPTu from cluster BH-GP-1A using Robertson's [8] method.

Table 2. Soil types of Schneider et al. [9] classification method.

Classification zones	Description of soil types
1a	Low I_r clays
1b	Clays
1c	Sensitive clays
2	Essentially drained sands and sand mixtures
3	Silts and transition soils

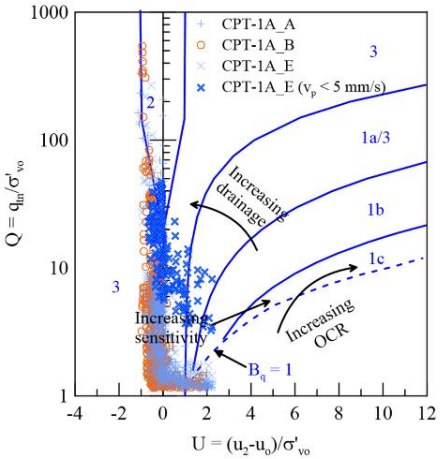

Figure 14a. Classiciation according to U − Q chart by Schneider et al. [9].

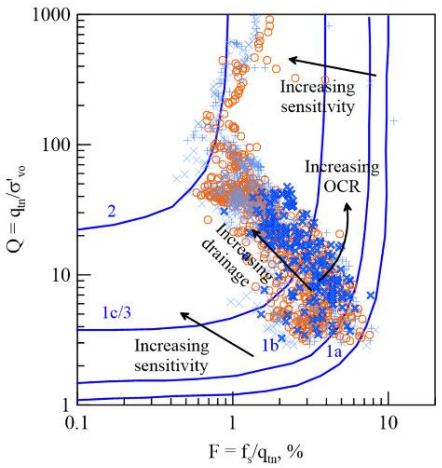

Figure 14b. Classiciation according to F−Q chart by Schneider et al. [9].

4.1. CPTu pore pressure dissipation tests

Partially drained and undrained cone penetration induces excess pore pressure around the cone tip. As soon as the cone penetration is suspended, the excess pore pressure starts to change. The rate of pore pressure change is related to the coefficient of consolidation of the surrounding soil. The dissipation test is conducted by recording the change of pore pressure while the cone penetration is suspended.

Four types of dissipation test behaviours can be identified [10][11] as illustrated in Fig. 15. For dissipation tests in clays, the pattern of pore pressure decay with time can be similar to Types I-III in Fig. 15. In heavily overconsolidated clays, CPTu induces negative pore pressure, the pore pressure at the beginning of dissipation test, u_i can be lower than u_o (Type III). In moderately overconsolidated clays, u_i can be higher than u_o (Type II). In Types II and III dissipation tests, the

measured pore pressure increases initially before decaying to u_o. In clays close to normal consolidation, u_i is usually higher than u_o and the pore pressure monotonically decreases with time before stabilizing to u_o (Type I). For dissipation tests in sands mixed with fines, the dissipation may have a behaviour similar to Type IV where u_i is lower than u_o and the pore pressure monotonically increases with time before reaching u_o.

Fig. 16 shows the change of u_2 with time during pore pressure dissipation tests in CPTu A at cluster BH-GP-1A or CPT-1A_A. The majority of the dissipation tests were of Type IV. The Type IV curves are marked in light greyish color in Fig. 16. Only a few dissipation tests in Fig.16 can be identified as Types I-III and they are marked with non-grey colors in Fig.16.

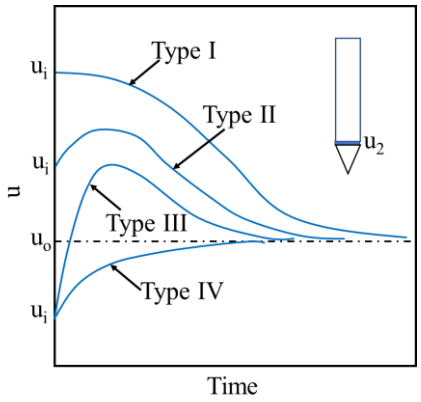

Figure 15. Types of u_2 dissipation tests results identified based on [10][11].

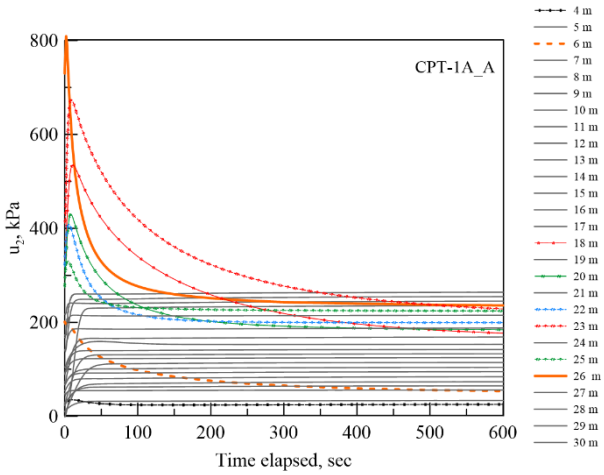

Figure 16. Time history of u_2 dissipation from CPT-1A_A pore pressure dissipation tests.

A total of 197 CPTu dissipation tests were conducted in this study; 62 were identified as Types I-III, 123 belonged to Type IV and 12 were discarded due to erratic dissipation behaviour related to testing issues.

A curve fitting procedure [12] was used to interpret Types I-III dissipation test data. In curve fitting the data, Λ = 0.8, $\emptyset'_{cs}$ = 30° and r = 17.8 mm (radius of cone) were set constant while I_r and OCR varied to obtain the best match between the measured and theoretical dissipation curve.

In analyzing Type IV dissipation data, the hydraulic conductivity in horizontal direction, k_h was estimated first using a correlation reported by [13] based on t_{50}. t_{50} is the time required for u_2 to reach 50% of the target value or $0.5(u_i - u_o)$. The correlation is simplified into an equation as follows,

$$k_h\{cm/s\} = \frac{1}{(251 \cdot t_{50})^{1.25}} \quad (9)$$

The Rowe cell test results on sand/silt mixtures were used to establish a correlation between k_h and c_h (or c_{ro}) as shown in Fig. 17. The horizontal coefficient of consolidation from CPTu dissipation test, c_{h-CPTu} was determined by a combination of Eq. 9 and Fig. 17.

Fig. 18 shows the c_{h-CPTu} values from all available CPTu pore pressure dissipation tests. There appears to be two groups of c_{h-CPTu}, which approximately match the high and low values of c_{ro} respectively, from Rowe cell tests shown in Fig. 5. This confirms that indeed c_{h-CPTu} reflects the compressibility in the radial or horizontal direction of the surrounding soil.

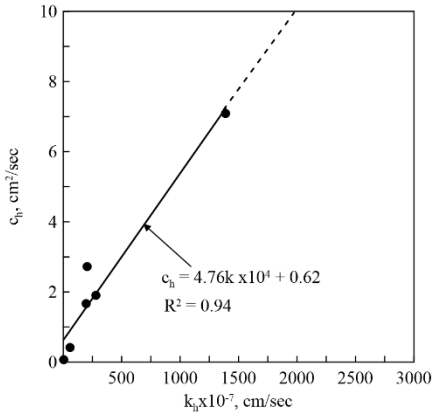

Figure 17. Correlation between k_h and c_h according to Rowe cell tests.

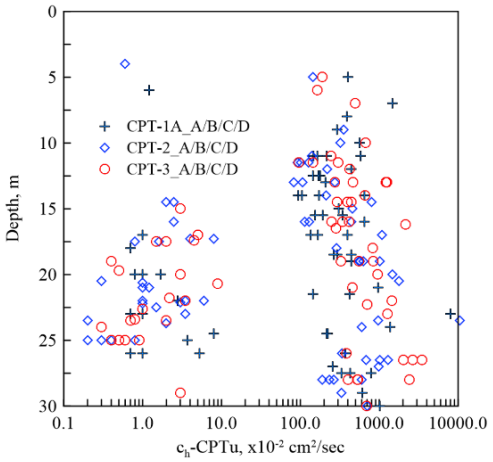

Figure 18. c_{h-CPTu} from available pore pressure dissipation tests.

4.2. Drainage condition based on normalized velocity

The c_{h-CPTu} measurements provided the key parameter needed to evaluate the drainage condition of cone penetration using the concept of normalized velocity, V [14] which is defined as

$$V = \frac{v_p \cdot d}{c_{h-CPTu}} \quad (10)$$

where

v_p = cone penetration rate

d = cone diameter (=35.6 mm for the cone used)

According to [15], V ranges between 0.03-0.01 and 30-100 for drained and undrained cone penetration, respectively.

Fig. 19 shows a correlation between V calculated using the c_{h-CPTu} from dissipation tests and I_C from the same depth where the dissipation tests were conducted. It appears that, when $I_C \geq 3$, V was consistently higher than 100, meaning that the CPTu was undrained. When I_C was between 2.6 and 3, V varied widely from less than 1 to 10000. It may thus be considered that when I_C was between 2.6 and 3, CPTu is partially drained. When $I_C <$ 2.6, V is mostly less than 10, CPTu is still partially drained but closer to fully drained condition.

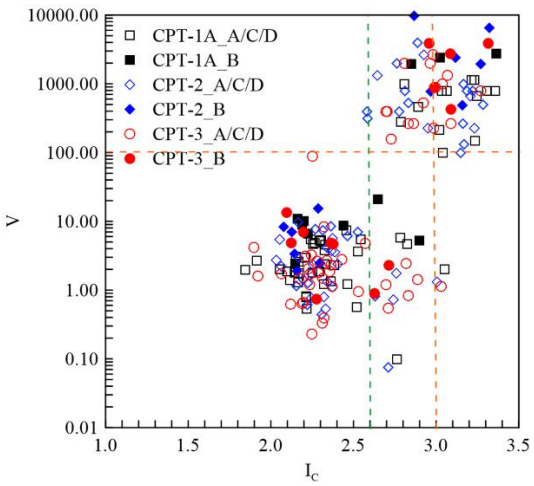

Figure 18. Correlation between V and I_C.

4.3. Estimating undrained shear strength from CPTu

With the knowledge of drainage and its relationship with CPTu, it is now possible to take advantage of the correlations that were developed originally for undrained CPTu, such as those to estimate undrained shear strength and OCR.

For undrained CPTu in clays, the following equation is often used to correlate q_t to undrained shear strength, s_u.

$$\frac{q_t-\sigma_{vo}}{N_{KT}} = s_u \quad (11)$$

N_{KT} is an empirical factor that may relate to soil plasticity and stress history. For applications that relate q_t to s_{u-DSS}, the above equation is modified as,

$$\frac{q_t-\sigma_{vo}}{N_{KT-DSS}} = s_{u-DSS} \quad (12)$$

where N_{KT-DSS} is dedicated for estimation of s_{u-DSS}. To validate Eq. (12), the s_{u-DSS} from DSS tests and those converted from s_{u-TX} as described above were used. Again, it was assumed that s_{u-DSS}/s_{u-TX} = 0.62. Three sets of consecutive CPTu records from type A CPTu performed at the same cluster as the DSS or TX were used to assess Eq. (12). The second CPTu record of the three was taken at depth comprarable to the middle of the DSS or TX specimen. An average of the three consecutive q_t values was used as the representative q_t to be used in Eq. (12). The lowest I_C from the three consecutive CPTu records, referred to as the I_{C-low} was used to represent the I_C for the depth range of the DSS or TX specimen. The I_{C-low} was chosen because a permeable layer can cause the nearby soil element to be more drained. Fig. 19 shows the correlation between N_{KT-DSS} and I_{C-low} using the available laboratory shearing test and field CPTu data. The results show that the lower I_{C-low} (CPTu became more drained) corresponds to higher N_{KT-DSS}. Although scattering still exists, the introdution of I_{C-low} helped quantifyng the effects of drainage so that a correlation between an undrained parameter such as s_{u-DSS} and a field measurement that may have variable degrees of drainage can be established. In this case, I_{C-low} was used as a factor that controls the magnitude of drainage adjustment.

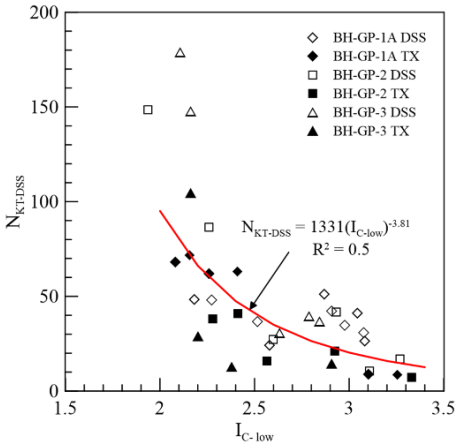

Figure 19. Correlation between N_{KT-DSS} and I_{C-low}.

4.4. Estimating OCR from CPT

Mayne [13] reported the following equation to estimate OCR using undrained CPTu in clays.

$$\text{OCR} = 2\left[\frac{(2/M)(q_t-\sigma_{vo})/\sigma'_{vo}}{(4/3)(lnI_r+1)+\pi/2+1}\right]^{(1/\Lambda)} \quad (13)$$

Considering the available TX and DSS results described above, Λ = 0.8, $\emptyset'_{cs}$ = 30°, I_r = 11.5 and data from A type CPTu at the three clusters (i.e., CPT-1A_A, CPT-2_A and CPT-3_A) were used in estimating OCR following Eq. (13). The results are shown in Fig.20, the hollow symbols came from all CPTu data within the depth range of 10 and 30 m. The hollow symbols scattered signifciantly with maximum OCR close to 100. The solid symbols came from "undrained" CPTu with $I_C \geq 3$.

Although with no distinctive trend, the range of OCR from 2 to 8 shown in Fig. 20 was surprsingly close to that estimated based on s_{u-DSS}/σ'_{vo} ratios (see Fig. 10). In this case, I_C was used as a filter to screen out CPTu data that were not undrained. The higher OCR values from undrained CPTu may be caused by the sand/silt contents in the soil and not related to stress history of the soil deposit.

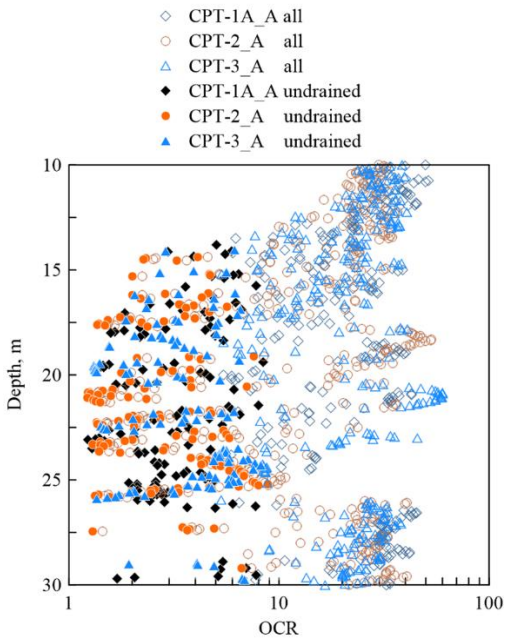

Figure 20. OCR from all CPTu data points and uundrained data points.

5. Conclusions

The series of CPTu and laboratory tests on high quality samples taken at the onshore test site provided data to evaluate the possibility of identifying the existence and effects of partial drainage on the interpretation of CPTu. This study demonstrates a procedure that can be used to select a threshold I_C value to distinguish undrained CPTu from partially drained CPTu, based on an extensive test programme with pore pressure dissipation tests and utilization of the concept of normalized velocity. Once this threshold I_C is established, empirical equations that were originally developed for undrained CPTu penetration can be applied by using I_C either as a drainage adjustment control factor or as a filter to exclude partially drained CPTus. It is very likely that the related empirical parameters reported herein are soil and site specific. A site specific calibration is imperative if the same method is to be applied for other locations.

Acknowledgement

The authors will like to thank the management of Ørsted for their kind permission to publish the work.

References

[1] Huang, A.B., Hsu, H.H., Chang, J.W. "The Behavior of a Compressible Silty Fine Sand," Canadian Geotechnical Journal, Vol.36, No.1, pp.88-101, 1999.

[2] Huang, A.B. & Huang, Y.T. "Undisturbed sampling and laboratory shearing tests on a sand with various fines con-tents," Soils and Foundations, Vol.47, No.4, pp.771-781, 2007.

[3] Huang, A.B., Tai, Y.Y., Lee, W.F., Ishihara, K. "Sampling and field characterization of the silty sand in central and southern Taiwan", I: The 3rd International Conference on Site Characterization, Taipei, 2008. pp.1457-1463, 2008.

[4] Huang, Y.T, Huang, A.B., Kuo, Y.C. & Tsai, M.D. "A laboratory study on the undrained strength of a silty sand from Central Western Taiwan," Soil Dynamics and Earth-quake Engineering, Vol.24, No.9-10, pp.733-743, 2004.

[5] Keaveny, J. and Mitchell, J.K. "Strength of fine-grained soils using the piezocone". Use of In-Situ Tests in Geotechnical Engineering, GSP 6, ASCE, Reston/VA, 668-685, 1986.

[6] Ladd, C.C., and Foott, R. "New design procedure for stability of soft clays," Journal of Geotechnical Engineering, ASCE, Vol.100, No.GT7, pp.763-786, 1974.

[7] Wroth, C.P., and Houlsby, G.T. "Soil mechanics – property characterization and analysis procedures," In Proceedings, 11th International Conference on Soil Mechanics and Foundation Engineering, San Francisco, Vol. 1, pp. 1–54, 1985.

[8] Robertson, P.K., "Cone penetration test (CPT)-based soil behaviour type (SBT) classification system – an update," Canadian Geotechnical Journal, Vol. 53, pp.1910-1927, 2016.

[9] Schneider, J.A., Hotstream, J.N., Mayne, P.W., and Randolph, M.F. "Comparing CPTU Q–F and Q–Δu_2 /σ'_{vo} soil classification charts," Géotechnique Letters, Volume 2, Issue 4, pp. 209-215, 2012.

[10] Sully, J.P., Campanella, R.G. "Evaluation of field CPTU dissipation data in overconsolidated fine-grained soils," Proceedings, XIII ICSMFE, New Delhi, 1994.

[11] Teh, C.I., and Houlsby, G.T. "An analytical study of the cone penetration test in clay," Géotechnique, 41(1): 17–34, 1991.

[12] Burns, S.E. and Mayne, P.W. "Monotonic and dilatory pore-pressure decay during piezocone tests in clay," *Can. Geotech. J.*, 35(6): 1063-1073, 1998.

[13] Parez, L. and Fauriel, R. "le piézocône améliorations apportées à la reconnaissance des sols," 1980.

[14] Finnie, I. and Randolph, M.F. "Punch-through and liquefaction induced failure of shallow foundations on calcareous sediments," Proc. Int. Conf. on Behavior of Offshore Structures, Boston (USA): 217-230, 1994.

[15] Randolph, M.F. and Hope, S. "Effect of cone velocity on cone resistance and excess pore pressures," *Proc. Int. Symp. on engineering practice and performance of soft deposits*, Osaka (Japan): 147-15, 2004.

[16] Mayne, P.W. "Interpretation of geotechnical parameters from seismic piezocone tests," Proceedings, CPT14, Paper #KN-2, Las Vegas, 2014.